Electrical, Control and Communication Engineering
ISSN 2255-9159 (online)
2025, vol. 21, no. 1, pp. 7–16
https://doi.org/10.7250/ecce-2025-0002
Published by RTU Press

Design of Helical Coil Gun Based on Self-Induction Coefficient and Projectile Size Optimisation

Hakan Citak (*Assoc. Professor, Balıkesir University, Balıkesir, Türkiye*),
Sabri Bicakci (*Assoc. Professor, Balıkesir University, Balıkesir, Türkiye*),
Huseyin Gunes (*Assoc. Professor, Balıkesir University, Balıkesir, Türkiye*),
Mustafa Coramik (*Assoc. Professor, Balıkesir University, Balıkesir, Türkiye*),
Yavuz Ege* (*Professor, Balıkesir University, Balıkesir, Türkiye*)

***Abstract* – Electromagnetic Launcher (EML) systems are classified into two main categories based on their fundamental operating principles: rail guns and coil guns. Rail guns accelerate a conductive projectile using magnetic force by passing a high current between two parallel rails, but they suffer from wear and heat accumulation due to mechanical contact. Coil launchers use electromagnets to accelerate ferromagnetic or conductive projectiles without contact, thus minimising energy losses and wear. Rail guns are preferred in military applications requiring high velocity and kinetic energy, whereas coil guns are more prominent in controlled acceleration applications such as space launch systems and laboratory experiments. Since the velocity of the generated electromagnetic field in coil launchers has no theoretical limit, the accelerated projectile also does not have a predefined velocity limit. However, the use of randomly sized coils and an increased number of sequential coils in coil guns disrupts the linearity of the projectile velocity increase. To address this issue, this study develops a "New Helical Coil Gun", consisting of four-stage helical coils designed to achieve linear velocity increase. First, the self-inductance coefficient of a coil was simulated based on the time-dependent variations of the current passing through it, and the inductance value that could provide a maximum instantaneous current of 25A (without direction change) under laboratory conditions was determined. Then, the design of the helical coil with a rectangular cross-section to provide this coefficient value was implemented. This design was then transferred to the ANSYS Maxwell magnetic analysis software, where an optimisation process was conducted to determine the ideal projectile size that would maximise the magnetic force exerted on a ferromagnetic projectile when a 25 A current was applied to the coil. Following this stage, a "Helical Coil Gun", composed of four-stage helical coils, was designed and manufactured based on the determined projectile and coil dimensions. Optical sensors were placed at the initial positions of the coils to measure the projectile's velocity. An FPGA-based project was developed for data acquisition, processing, and triggering control. This project, designed using the LabVIEW FPGA module, was carried out on the NI myRIO-1950 board containing Xilinx FPGA. After each launch, the collected data was stored on a flash drive connected to myRIO and monitored in real time via a display. What distinguishes this study from literature is its approach to determining the optimal coil geometry by correlating the current variation characteristics with the coil's self-inductance coefficient and using Genetic Algorithm-based optimisation to identify the ideal projectile size that achieves maximum velocity under maximum force. Experiments with the developed coil gun showed that the projectile velocity change from the beginning of the first coil to the end of the fourth coil was linear.**

***Keywords* — Ferromagnetic projectile, FPGA, genetic algorithm, Helical coil gun, LabVIEW.**

I. Introduction

Electromagnetic launch systems are categorised into various sub-classes based on their operating principles. Inductive launchers (IND) generate a contactless thrust force by creating a magnetic field through coils, while direct connection launchers (DIR) aim to achieve high velocities by transmitting electric current directly to the projectile in rail systems. Electrothermal-chemical (ETC) launchers generate thrust by combining electromagnetic energy with chemical reactions, whereas magnetoplasmadynamic (MAG) systems accelerate high-temperature plasma using magnetic fields. Electrostatic (EST) launchers accelerate light particles using high-voltage electric fields, and hybrid (HYB) systems aim to increase efficiency in military and space applications by combining multiple thrust methods [1]–[3].

Magnetic launch systems have become a significant alternative in the aerospace and defence industries compared to traditional mechanical launch methods, offering higher energy efficiency and precise control over thrust force [4], [5]. Superconducting magnetic bearings and permanent magnet linear motors enhance the structural integrity of launch systems while enabling launch platforms to provide a more stable magnetic environment [6], [7]. However, issues such as the magnetic field distribution and thermal management of electromagnetic launchers still require comprehensive analysis [8]–[10].

New design approaches optimise magnetic flux lines, thereby increasing the launcher's exit velocity and allowing for high efficiency even at low operating voltages [11]–[13]. Furthermore, different electromagnetic coil configurations and multipolar field mechanisms contribute to the development of high-precision and long-range launch systems by improving

* Corresponding author. E-mail: yege@balikesir.edu.tr
Received 05-11-2025, accepted 12-02-2026

acceleration during launch [14]–[17]. New methods, such as sensorless position detection supported by artificial intelligence, also enhance the accuracy and system efficiency of the electromagnetic launchers [18].

Coil guns and rail launchers used in electromagnetic launch systems generate stronger and more stable thrust forces through various engineering solutions. For instance, copper-steel composite rails improve the contact conditions between the armature and the rail, resulting in a more balanced current distribution [19]. Additionally, four-pole rail launchers and series-connected electromagnetic propulsion systems enhance launch efficiency by providing higher electromagnetic thrust forces [20], [21].

Moreover, advanced magnetic modelling techniques and intelligent algorithms optimise the design process of electromagnetic launch systems, enabling more accurate analysis of various physical parameters [22]–[24]. Research on the energy management and power supply systems of electromagnetic launchers enhances overall system performance by reducing charging times and improving cycle durations [25], [26].

The use of randomly sized coils and an increased number of sequential coils in coil guns disrupts the linearity of projectile velocity increase. In this context, a "New Helical Coil Gun" consisting of four-stage helical coils has been developed in this study, aiming to achieve maximum linear velocity increase. To reach this goal, the optimal coil geometry was determined by relating the current variation characteristics to the self-inductance coefficient of the coil. Furthermore, through optimisation using Genetic Algorithms, the ideal projectile size that ensures maximum velocity based on maximum force was identified. This makes the present study different from the existing literature.

II. Material and Method

In the study, the energization circuit of the coils in the helical coil gun to be developed has been first designed. As shown in Fig. 1, it is aimed to switch the capacitor loaded with a DC power supply via a thyristor and discharge it through the coil.

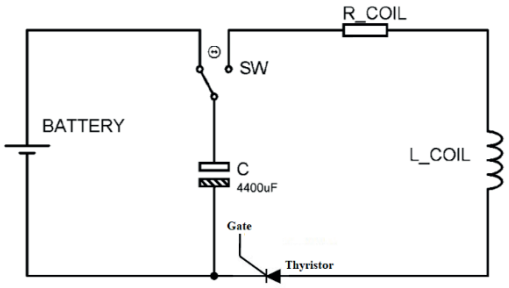

Fig. 1. Coil energization circuit.

When the coil is energized, the current flowing through it can be found by (1).

$$\alpha = \frac{R_{\text{coil}}}{2 \times L_{\text{coil}}}.$$

$$\beta = \sqrt{\alpha^2 - \frac{1}{L_{\text{coil}} \times C}}.$$

$$A_1 = \frac{V_0}{2 \times \beta \times L_{\text{coil}}}.$$

$$A_2 = -\frac{V_0}{2 \times \beta \times L_{\text{coil}}}.$$

$$i_L = e^{-\alpha t} \times \left(A_1 \times e^{\beta t} + A_2 \times e^{-\beta t} \right). \quad (1)$$

As seen in (1), the self-induction coefficient of the coil plays an important role in the time variation of the current passing through the coil. Therefore, the dependence of the time variation of the current flowing through the coil on the self-induction coefficient was investigated (Fig. 2).

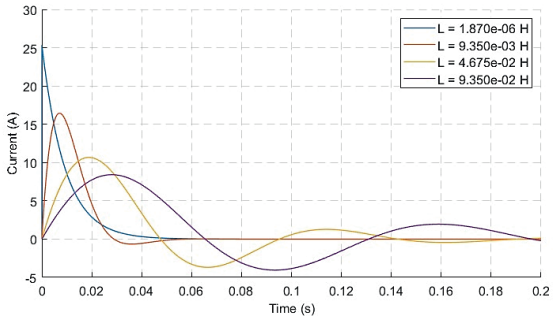

Fig. 2. The effect of the self-induction coefficient on the current passing through the coil.

As shown in Fig. 2, the increase in the self-induction coefficient of the coil not only reduces the passing current but also reverses its direction. This means that the force acting on the projectile changes direction, and the projectile is slowed down. Therefore, in this study, the ideal value of the induction coefficient was determined according to the highest current that could be provided under laboratory conditions. In the laboratory where the study was carried out, it was found that the value of the induction coefficient of the coils in the helical coil gun to be developed considering the 25 A limit should be 1.87 µH (Fig. 2). Then, the ideal geometrical properties of the coil were determined using (2), which gives the induction coefficient of a rectangular cross-section helical coil (Fig. 3) [27].

$$L_{\text{COIL}} = 0.002 \times \pi^2 \times \left\lfloor \frac{2a}{b} \right\rfloor \times n^2 \times a \times \left(K - k \right),$$

$$L_{\text{COIL}} = 0.002 \times \pi^2 \times \left\lfloor \frac{2a}{b} \right\rfloor \times n^2 \times a \times K' \quad . \quad (2)$$

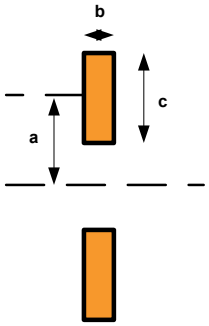

Fig. 3. Cross-section of the coil.

K' in (2) is a factor that depends on the ratio ($2a/b$) and also on the dimensions of the cross-section. To determine a, b, c, n values that will provide the self-induction coefficient of 1.87 µH, these values were kept variable, and the value of K' for each a, b, c value was determined by the "Grover tabular calculation method" [27], [28]. In this way, a, b, c, n, and K' values that gave the closest result to 1.87 µH among the L values determined by (2) were found to be 7.25 mm, 2 mm, 7.5 mm, 13, 0.106, respectively.

After this stage, the coil whose geometrical properties were determined was modelled in ANSYS Maxwell (Fig. 4). The aim of this modelling is to find the variation of the force acting on the projectile when 25 A is applied to the coil according to the projectile size and to optimise the projectile size.

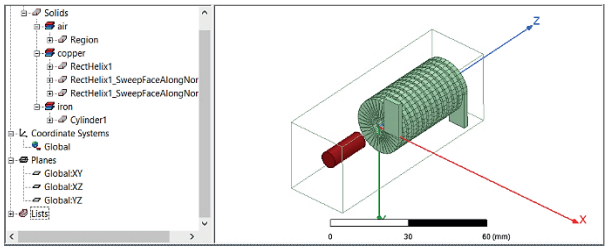

Fig. 4. ANSYS Maxwell model of the geometrically characterised coil.

In this study, the Genetic Algorithm is preferred for projectile size optimisation. This is because Genetic Algorithm gives successful results for problems such as parameter and system identification, control systems, and engineering designs in addition to other optimisation methods (Quasi Newton, Adaptive Multiple Objective, etc.) [29]. In addition, the Genetic Algorithm can converge to the global optimum without getting stuck in local minimum in nonlinear, multimodal, and complex problems. It provides better results by scanning the solution space in a wide scope and offers the flexibility to work with both continuous and discrete variables. Accordingly, in this study, the cylindrical projectile was optimised, and boundary values for diameter, height, and projectile position were determined. Since the inner diameter of the coil is 3.5 mm, the maximum limit value of the projectile diameter is selected as 3.4 mm, and the maximum value of the projectile height is selected as 18 mm since the magnetic force changes direction after the centre point of the 38 mm long coil. Considering the position where the magnetic force changes direction (+10 mm), the optimisation was decided to be between –20 mm and +15 mm (Fig. 5a). In the analysis of the model under these optimisation conditions, 25 A was applied to the coil and optimisation was performed in 680 iterations. As a result of the optimisation, it was found that the maximum magnetic force was generated when the projectile diameter was 3.4 mm, and the projectile length was 18 mm when the projectile was at –5 mm (Fig. 5b).

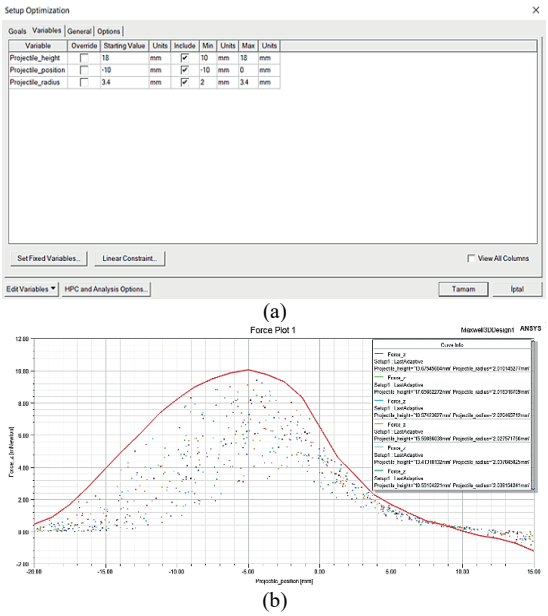

Fig. 5. (a) Optimisation setup, (b) optimisation result at 680 iterations.

In the next step, the limits of the projectile position in the optimisation were determined between –10 mm and 0 mm, based on the position where the maximum force occurs (Fig. 5b). The optimisation process was repeated for 400 iterations. Thus, the number of iterations in this region was increased, and it was confirmed that the maximum magnetic force was generated at the same projectile diameter (3.4 mm) and projectile length (18 mm) (Fig. 6a). This is also seen in the graph of the magnetic force variation with respect to the projectile position plotted for four different iterations (Fig. 6b).

As shown in Fig. 6b, although the projectile diameter and projectile height change in the iteration, the magnetic force acting on the projectile starts at –25 mm, reaches its maximum value at –5 mm, and decreases to zero at +10 mm. Then it changes direction. Therefore, the instantaneous 25 A current to be applied to the coils must be applied when the projectile is at –30 mm and must be completely damped when it reaches +10 mm. Otherwise, since the direction of the force changes after +10 mm, the projectile will slow down. To avoid this situation, it is necessary to determine how long it takes for the projectile to reach from –30 mm to +10 mm for the first coil. As it is known, the work done by the magnetic force is equal to the kinetic energy change of the projectile. However, since the magnitude of the magnetic force changes with position between these positions, it is necessary first to find the position-dependent equation of the magnetic force, then determine the work provided to the projectile using (3), and

then determine the final velocity of the projectile using (4) when the projectile reaches +10 mm.

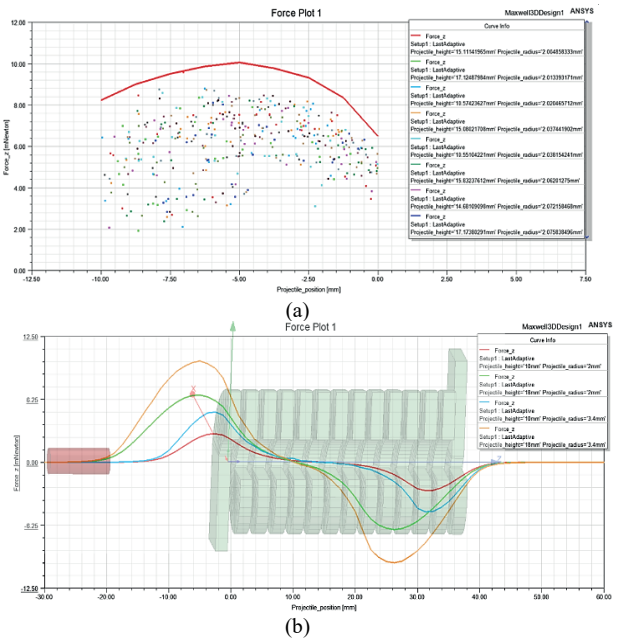

Fig. 6. (a) Optimisation result at 400 iterations, (b) Variation of magnetic force with respect to projectile position for four selected iterations.

In this case, the initial velocity, the final velocity, and the average acceleration values to be determined with the work information can be used in the time-dependent velocity equation to find out how long it takes the projectile to reach +10 mm. However, if the friction of the air is taken into account, there may be a minor error (1–2 %) in this theoretically determined time value. However, a coil gun consisting of four coils in a row is considered in the study and, therefore, the projectile will enter each coil at a higher velocity than the previous one. This will cause the coil transition time to become shorter and shorter. For the energy transferred to the projectile to be the same in each coil and the velocity increase to be implemented linearly, the damping time of the current in each coil should be shorter than the calculated transition time.

$$W = \int_{x_1}^{x_2} F \mathrm{d}x \tag{3}$$

$$\upsilon = \sqrt{\frac{2 \times W}{m_p}} \tag{4}$$

In this direction, the force-position graph was fitted using Origin data analysis software to determine the position-dependent equation of the magnetic force. The equation obtained in this way and the constant values of this equation are provided in Fig. 7. Among these constants, the value of A is equal to the area under the force curve, and this also gives the work provided to the projectile (1.57×10^{-3} J).

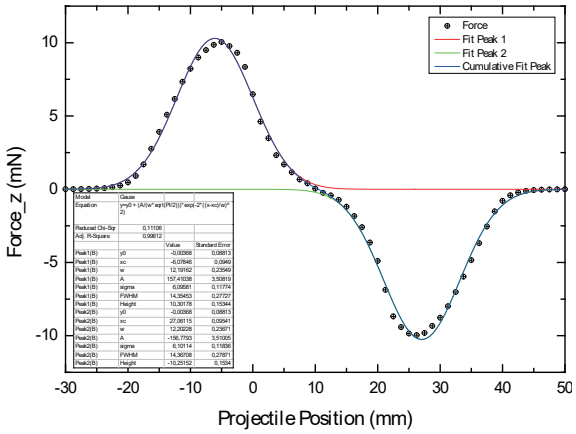

Fig. 7. Fit curve of magnetic force-position variation.

In the study, the average acceleration value (4.717 m/s^2), the initial velocity, and final velocity information were obtained with the direct work information determined in this way. The initial velocity, final velocity, projectile mass (8.48 g), and average acceleration information were used to find out the application times of the force for each coil. Table I provides the results obtained when the initial velocity of the projectile was selected as zero at the beginning of the first coil and the time of application of the force for each coil. During the calculations, air resistance was neglected in the distance between the coils where the projectile was not subjected to magnetic force, and it was assumed that the velocity remained constant.

TABLE I
THE FORCE APPLICATION TIME CALCULATED FOR EACH COIL AT ZERO PROJECTILE ENTRY VELOCITY
(–30 mm to +10 mm range)

	1st Coil	2nd Coil	3rd Coil	4th Coil
υ_{Input}	0	0.616 m/s	0.871 m/s	1.066 m/s
υ_{Output}	0.616 m/s	0.871 m/s	1.066 m/s	1.231 m/s
Force Application Time	0.129 s	0.053 s	0.040 s	0.034 s

If the projectile input velocity of the first coil is different from zero, the application times of the force given in Table I will decrease slightly. When the curve given in blue in Fig. 2 is examined, it is evident that the current of 25 A in the selected coil is damped at approximately 0.03 s. If the friction of the air is also taken into account, the current passing through the coil will be damped when the projectile reaches +10 mm. In this case, it can be stated that the projectile is only under the effect of an accelerating magnetic force. This is also the same for the four coils in the coil gun. Therefore, in the coil gun to be developed with the determined properties, the energy gained by the projectile in the coils energized sequentially will be the same and thus the velocity of the projectile will increase linearly.

III. Experimental Verification

At this stage of the study, the helical coils of the new helical coil-gun system to be developed have been first manufactured (Fig. 8). Technical information of the helical coil is provided in Table II.

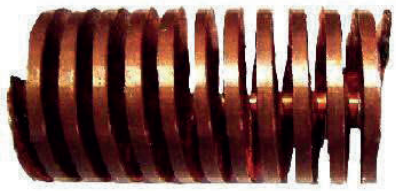

Fig. 8. Helical coil.

TABLE II
Technical Information on the Helical Coil

Winding width	Distance between windings	Coil length	Inside diameter	Outer diameter	Number of windings
2 mm	1 mm	38 mm	3.5 mm	11 mm	13

After the production of the four helical coils was completed, the coils were placed sequentially in a compact structure made of castermid and brass shaft with a distance of 40 mm between them (Fig. 9). At the inlet of each coil, IR optical transceiver sensors were mounted, positioned opposite to each other, for energizing the coils and measuring the velocity. In addition, one of the same sensors was placed at the output of the 4th coil to determine the exit velocity of the projectile from the coil. The sensors react to state changes (rise and fall time) within 100 ns and produce logic 1 or logic 0 output. This fast response time is sufficient to measure the velocity of a projectile traveling at high velocity.

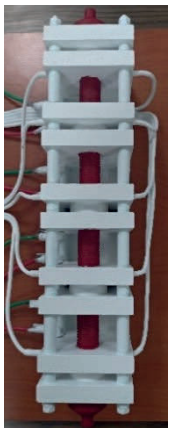

Fig. 9. Mechanics of the developed helical coil-gun system.

In the next stage of the study, the projectile with the dimensions determined as a result of optimisation and with a Fe content of 88.016 % was manufactured. X-ray diffraction (XRD) results of the projectile are illustrated in Fig. 10.

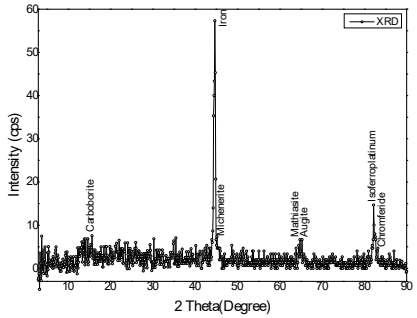

Fig. 10. XRD results of the projectile.

NI's myRIO embedded system was used to process the data from the velocity and trigger sensor sets, energize the coils, and record the data. myRIO platform's FPGA-based programmable logic system has a processing velocity of 25 samples/ns. This processing velocity is much less than the time it takes for the projectile to reach the energization point of the next coil. Table III shows the sensor connection points to the myRIO platform.

TABLE III
Connection Points of Sensors to myRIO Platform

Sensor / Coil	myRIO I/O port
Velocity Sensor - S1	Connector A - DI0
Velocity Sensor - S2	Connector A – DI1
Velocity Sensor - S3	Connector A – DI2
Velocity Sensor - S4	Connector A – DI3
Velocity Sensor - S5	Connector A – DI4
Trigger for Coil 1 - C1	Connector A – DO5
Trigger for Coil 2 - C2	Connector A – DO6
Trigger for Coil 3 - C3	Connector A – DO7
Trigger for Coil 4 - C4	Connector A – DO8

Initially, all sensor outputs are logic 1 since there is no projectile in front of them. When the projectile, moving with a small external force, reaches the front of the S1 velocity sensor at time t_1, the sensor output drops to logic 0, and the t_1 value is stored in memory with a precision of 1 µs. When the projectile leaves the front of the S1 sensor at time t_2, the sensor output returns to logic 1, and the t_2 value is also stored in memory. Subsequently, the time interval Δt ($\Delta t = t_2 - t_1$) is calculated, and the projectile's velocity is determined in m/s and recorded. The signal variation at the S1 sensor based on the projectile's position is shown in Fig. 11.

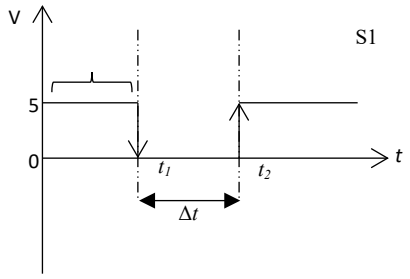

Fig. 11. Signal change in the S1 sensor according to the position of the projectile.

After the first coil is energized, depending on the position of the projectile, signal changes occur in sensors S2, S3, and S4, respectively, and the projectile reaches its final velocity by energizing the last helical coil. Finally, the velocity measurement procedure is repeated at the S5 velocity measurement sensor, thus completing the magnetic launch process. In the developed helical coil-gun system, the final version of the power circuit, which provides the energization of each helical coil and is shown in Fig. 1, integrated with the myRIO is presented in Fig. 12.

As shown in Fig. 12, due to the pulse from myRIO, the current flowing through the primary winding of the pulse transformer ZKB421/09 causes a voltage drop in the secondary winding. When the primary voltage is 15 V, the secondary voltage can reach 125 V. The 14 Ω resistor on the secondary side is used to limit the gate current of the thyristor. In addition, the R-C turn-off snubber circuit in the energization circuit is designed to prevent voltage oscillations and sudden voltage spikes that may occur during energization at the helical coil and DSEI-60-12 fast diode terminals.

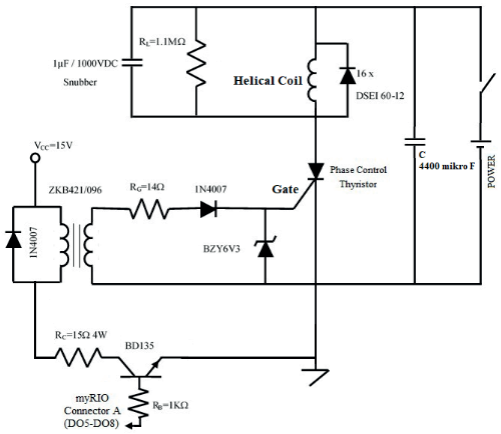

Fig. 12. Helical coil energization circuit.

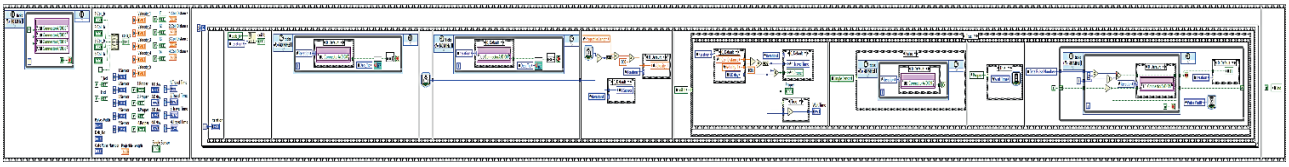

Fig. 13. FPGA program developed for the helical coil gun.

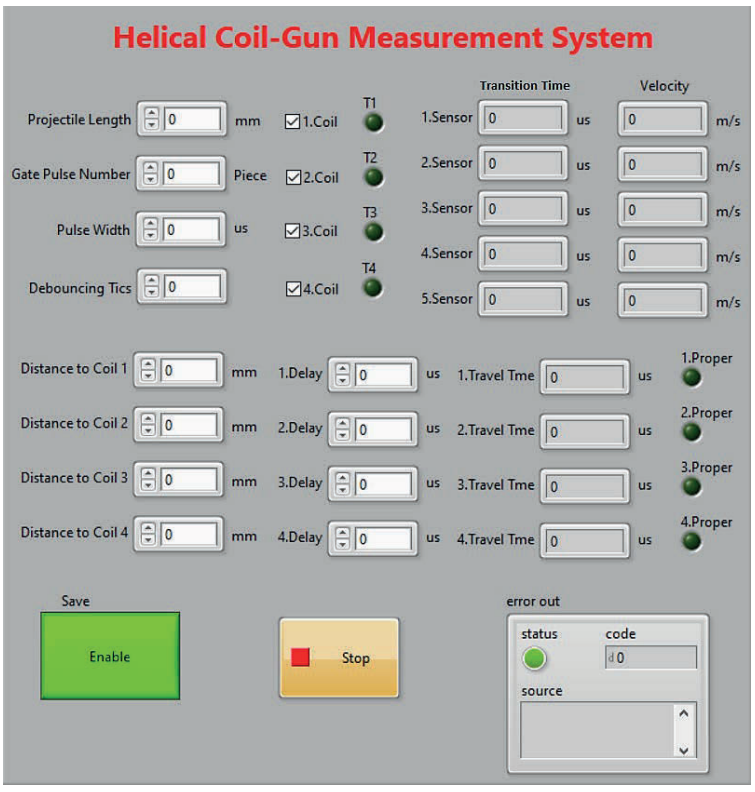

Fig. 14. Front panel of the user interface program developed for the helical coil gun.

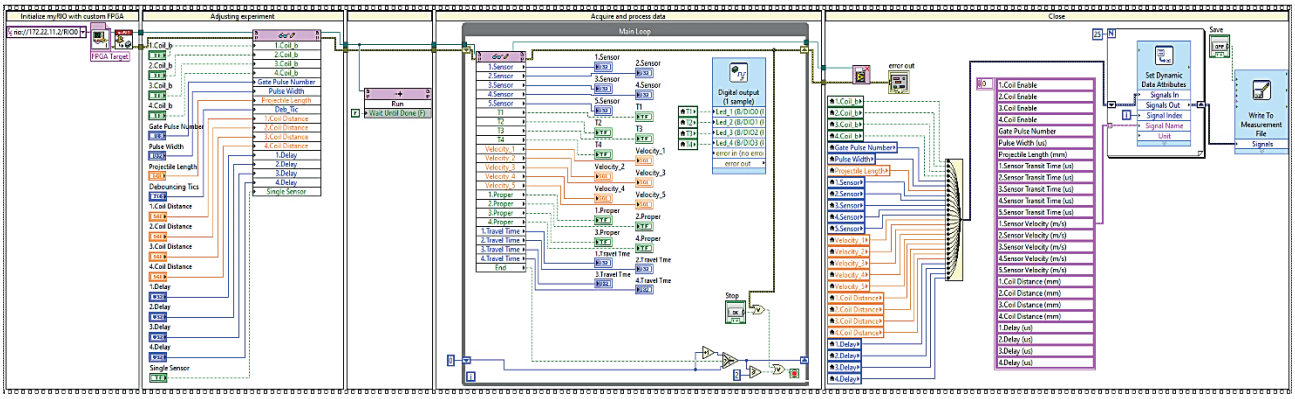

Fig. 15. Block diagram of the user interface program developed for the helical coil gun.

In addition, a graphical FPGA program was developed using LabVIEW to trigger the transistor and energize the coils (Fig. 13). For the FPGA control software to work interactively with the user and for the data to be saved to the USB on myRIO, a graphical-based program running on the ARM A9 processor of myRIO was created. The front panel and block diagram screenshots of this program are demonstrated in Figs. 14 and 15, respectively.

When the LabVIEW-based software shown in Fig. 14 is run, the first step is selecting the data recording file. Then, the projectile length, number of gate pulses, pulse width, and debouncing tics values are entered to ensure stable operation of the system. Finally, in order to minimise the effect of air friction, the distance at which the energization trigger is applied to the coil and, if necessary, the setting of an additional delay time are provided through the inputs on the interface. Thus, it is aimed to achieve maximum and linear velocity. Upon launch, the Δt value calculated by myRIO for each coil, representing the projectile's transition time, along with the velocity computed using this time, is transmitted to the interface screen via the USB port and stored in myRIO's flash memory. Additionally, the presence of the trigger signal reaching myRIO can be monitored through LED indicators on the interface. A photograph of the helical coil-gun system developed in this study is presented in Fig. 16.

Fig. 16. The developed helical coil-gun system.

While testing the launch performance of the helical coil-gun system developed in the experimental phase of the study, 4400 μF capacitors were loaded by applying 53 V DC voltage, and the energy circuit was set to allow 25 A damped current to pass through the helical coils when triggered. Then, the projectile length (18 mm), gate pulse number (1), pulse width (100 μs), and debouncing tics (3) were entered from the user interface, and other values, such as distance to the coil and delay time, were kept variable for maximum and linear velocity experiments. The initial entry velocity of the projectile was varied by a mechanical system to 0.20 m/s, 0.40 m/s, 0.50 m/s, and 0.55 m/s. Some experimental results from more than 100 experiments varying the distance to the coil and delay time at each input velocity are provided in Table IV. In addition, according to these results, the velocity-time graphs of the projectile for each input velocity were drawn (Fig. 17).

According to Table IV, as the projectile's entry velocity increases, the duration of exposure to the magnetic force, particularly in the 4th coil, decreases. When the projectile entry velocity is more than 0.55 m/s, although the exit velocity of the projectile from the coil gun increases, the transition time of the projectile, especially from the 3rd and 4th coil to the distance where the force is applied, decreases below 0.03 s. Since this time is less than the damping time of the current, the linear velocity increase of the projectile is disturbed. It can be stated that the reason for this situation is that not all the work provided by the magnetic force can be transferred to the projectile as kinetic energy. The linear velocity increase of the projectile means that the range can also be adjusted with this helical coil gun.

Furthermore, in systems that provide a gradual increase in velocity, such as the developed helical coil gun, it has been determined that the state change durations of the sensors (100 ns) and the processing times of FPGA-based programmable logic systems (25 ns) are negligible in achieving linear velocity in the projectile. On the contrary, the importance of the induction coefficient values of the coils to be selected in such coil guns has emerged. It has been determined that changing the damping time of the current by changing the induction coefficient has a great effect on obtaining the linear velocity in the projectile. However, the decrease in the time of

application of the magnetic force with a gradual increase in velocity limits the number of coils in the coil gun and thus the projectile exit velocity. In short, even if the self-induction coefficients of the coils to be used in the coil gun are adjusted, the linear increase of the projectile velocity will be disturbed by increasing the number of coils. Of course, when the number of coils increases, the exit velocity will increase, but since the linearity of the velocity is disturbed, range adjustment will not be possible.

If the magnitude of the work done by the magnetic force is found theoretically, as in this study, it can be determined how many coils the projectile is exposed to the force, and the damping time of the current will be equalized. Considering this situation, the number of coils was selected as four in this study. Thus, until the projectile entry velocity is 0.55 m/s, the velocity increase provided by all coils to the projectile is equal and a linear velocity-time change is obtained for the projectile (Fig. 17).

TABLE IV
SOME EXPERIMENTAL RESULTS OBTAINED USING THE DEVELOPED HELICAL COIL-GUN SYSTEM

	Voltage (V)	**Current (A)**	**Input Velocity (m/s)**		**1st Coil**	**2nd Coil**	**3rd Coil**	**4th Coil**	**υ_{Output}**
Capacitor (4400 μF)	53	25	0	Force Application Time (s)	0.13023	0.05394	0.04139	0.03490	
				Velocity (m/s)	0.61430	0.86875	1.06399	1.22859	1.22758
			0.2	Force Application Time (s)	0.09129	0.05129	0.04015	0.03414	
				Velocity (m/s)	0.64603	0.89147	1.08262	1.24476	1.24374
			0.4	Force Application Time (s)	0.06477	0.04521	0.03701	0.03214	
				Velocity (m/s)	0.73305	0.95641	1.13670	1.29207	1.29106
			0.5	Force Application Time (s)	0.05568	0.04184	0.03509	0.03085	
				Velocity (m/s)	0.79206	1.00236	1.17562	1.32644	1.32541
			0.55	Force Application Time (s)	0.05191	0.04019	0.03501	0.03017	
				Velocity (m/s)	0.82454	1.02821	1.19774	1.34608	1.34502

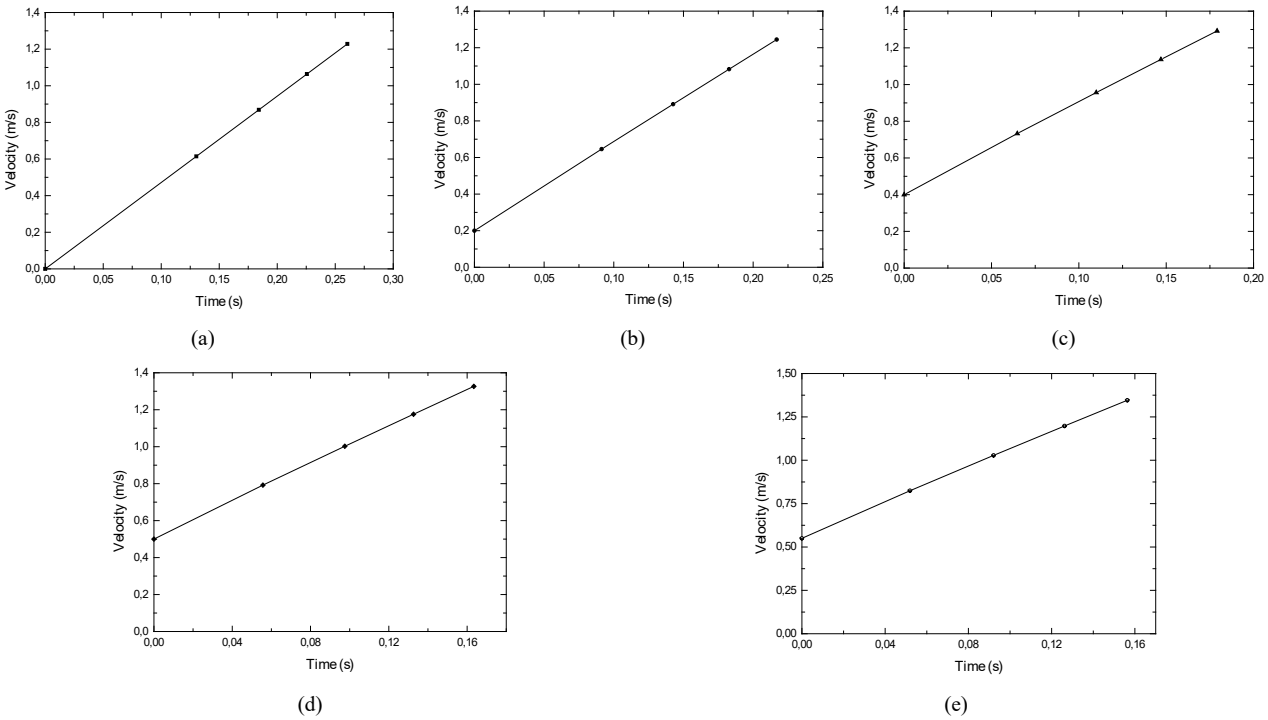

Fig. 17. Experimentally determined projectile velocity-time variations for (a) 0 m/s, (b) 0.2 m/s, (c) 0.4 m/s, (d) 0.5 m/s, (e) 0.55 m/s.

IV. CONCLUSION AND RECOMMENDATION

In this study, a new coil gun consisting of four stages of helical coils was designed and manufactured to ensure that the velocity increase in coil guns remains linear. As a result of simulation and experimental studies, it was found that the determined induction coefficient and coil geometry were optimised to provide maximum force to the projectile with the applied current. The tests have shown that an uncontrolled

increase in the number of coils disrupts the linear increase in velocity and therefore makes range adjustment difficult. In this study, it was predicted that the number of coils in a coil gun could be increased until the projectile's exposure time to the magnetic force equalled the current decay time, thereby achieving a linear increase in velocity. Using theoretical calculations of the work done by the magnetic force, the projectile's exposure time to the magnetic force was determined, leading to the decision to develop a four-coil system. Experimental tests conducted after the manufacturing of the coil gun confirmed that the projectile's velocity change remained linear up to an initial velocity of 0.55 m/s.

Based on the findings, the following suggestions are provided for the design of coil-gun systems.

1. Optimisation of the Coefficient of Induction: The correct determination of the self-induction coefficient of the coils allows the damping time of the current to be controlled, linearizing the velocity increase of the projectile. For this reason, it should be kept in mind that the magnetic properties of the projectile should also be taken into account in the design phase in order not to disturb the linearity in the velocity.
2. Limiting the Number of Coils: In order to maintain the continuity of the magnetic force applied to the projectile, the number of coils must be increased to the point where the damping time of the current and the residence time of the projectile in the coil are compatible. Otherwise, the velocity increase will not be linear.
3. Control of Initial Velocity: The initial velocity of the projectile must be kept within a range where the system can provide linear velocity increase. In the study, a linear velocity increase up to 0.55 m/s was obtained; therefore, the design should be made taking into account the sensitivity of the coil guns to the initial velocity.
4. Advantages of FPGA Based Control: The use of FPGA-based systems in real-time data processing and triggering processes ensures that the response time of sensors and logic circuits remains negligible. For this reason, it is recommended to continue the use of FPGA in coil-gun systems that require high velocity and precision.
5. Increasing the Maximum Output Velocity and Range: By increasing the number of coils, the output velocity increases; however, this situation disrupts the linear velocity increase and makes range control difficult. Therefore, the velocity-range balance should be optimised according to the intended use of the system.

As a result, the developed helical coil-gun system offers a more predictable and controllable velocity profile compared to the randomly sized and multistage coil-gun systems in the literature. Future studies can focus on improving the performance of the system through more efficient energy transfer mechanisms and different coil geometries.

REFERENCES

[1] T. G. Engel, "Scientific classification method for electromagnetic launchers," *IEEE Transactions on Plasma Science*, vol. 45, no. 7, pp. 1333–1338, May 2017. https://doi.org/10.1109/TPS.2017.2705177

[2] T. G. Engel, J. M. Neri, and M. J. Veracka, "The maximum theoretical efficiency of constant inductance gradient electromagnetic launchers," *IEEE Transactions on Plasma Science*, vol. 37, no. 4, pp. 608–614, Feb. 2009. https://doi.org/10.1109/TPS.2009.2014379

[3] T. G. Engel and M. J. Veracka, "The voltage-current scaling relationship and impedance of DC electromagnetic launchers," *IEEE Transactions on Plasma Science*, vol. 43, no. 5, pp. 1271–1276, Apr. 2015. https://doi.org/10.1109/TPS.2015.2418053

[4] A. Sibilska-Mroziewicz, E. Ładyżyńska-Kozdraś, and K. Sibilski, "VR-supported analysis of UAV – magnetic launcher's cart system," *Energies*, vol. 16, no. 10, May 2023, Art. no. 4095. https://doi.org/10.3390/en16104095

[5] E. Ładyżyńska-Kozdraś, A. Sibilska-Mroziewicz, K. Sibilski, D. Potoka, and A. Żyluk, "Dynamics of separation of unmanned aerial vehicles from the magnetic launcher cart during takeoff," *Electronics*, vol. 12, no. 13, June 2023, Art. no. 2883. https://doi.org/10.3390/electronics12132883

[6] S. Basaran, M. Altinkilic, and S. Sivrioglu, "A linear motor launcher system integrating a multisurface superconducting magnetic bearing," *IEEE Transactions on Applied Superconductivity*, vol. 33, no. 6, pp. 1–7, May 2023. https://doi.org/10.1109/TASC.2023.3275303

[7] G. Li, X. Wang, P. Cui, and J. Li, "Analysis of superconducting linear synchronous motor for electromagnetic propulsion," *Cluster Computing*, vol. 22, pp. 2709–2717, Jan. 2018. https://doi.org/10.1007/s10586-017-1434-y

[8] S. Ozkucuk and M. C. Kulahli, "Solar photovoltaic source based magnetic launcher simulation design with thermal requirements consideration," *Renewable Energy*, vol. 145, pp. 1004–1013, Jan. 2020. https://doi.org/10.1016/j.renene.2019.06.073

[9] S. Guan, X. Guan, J. Shi, and B. Wu, "Numerical analysis and measurement of high in-bore magnetic field of synchronous induction coil launcher," *IEEE Access*, vol. 10, pp. 3447–3458, Dec. 2021. https://doi.org/10.1109/ACCESS.2021.3139672

[10] M. Ma, T. Wei, Z. Xu, Z. Xu, H. Li, and W. Qunjing, "Electromagnetic interference analysis of permanent magnet linear synchronous launchers," *IEEE Transactions on Plasma Science*, vol. 48, no. 5, pp. 1309–1315, Apr. 2020. https://doi.org/10.1109/TPS.2020.2983472

[11] M. M. M. Abdo, H. El-Hussieny, T. Miyashita, and S. M. Ahmed, "Design of a new electromagnetic launcher based on the magnetic reluctance control for the propulsion of aircraft-mounted microsatellites," *Applied System Innovation*, vol. 6, no. 5, Sep. 2023, Art. no. 81. https://doi.org/10.3390/asi6050081

[12] B. Cheng, "The design and simulation of a novel electromagnetic launcher with permanent magnet," in *2022 7th International Conference on Mechanical Engineering and Robotics Research (ICMERR)*, Krakow, Poland, Dec. 2022, pp. 114–117. https://doi.org/10.1109/ICMERR56497.2022.10097818

[13] I. R. McNab, "Brief history of the EML symposia: 1980–2018," *IEEE Transactions on Plasma Science*, vol. 47, no. 5, pp. 2136–2142, Dec. 2018. https://doi.org/10.1109/TPS.2018.2885269

[14] S. Kondamudi and M. R. Pasumarthi, "Computations of magnetic forces in multipole field electromagnetic launcher," *International Journal of Mathematical, Engineering and Management Sciences*, vol. 4, no. 3, Apr. 2019, Art. no. 761. https://doi.org/10.33889//IJMEMS.2019.4.3-059

[15] K. Manohar and K. Srichandan, "Analysis of quadrupole magnetic field reluctance-based launcher with different coil switching patterns," *IEEE Transactions on Plasma Science*, vol. 51, no. 5, pp. 1370–1376, Apr. 2023. https://doi.org/10.1109/TPS.2023.3266515

[16] S. Boisseau *et al*., "An autonomous switch based on a rotating magnet driven by magnetic launchers," *Smart Materials and Structures*, vol. 30, no. 2, Jan. 2021, Art. no. 02LT01. https://doi.org/10.1088/1361-665X/abd7e8

[17] H. Deng, Y. Wang, G. Fan, L. Liang, and Z. Yan, "Design and test of a single-stage double-layer multipole field electromagnetic launcher with a rotational performance," *IEEE Access*, vol. 7, pp. 112008–112014, Aug. 2019. https://doi.org/10.1109/ACCESS.2019.2935111

[18] O. Çetin, H. Özbay, A. Dalcalı, and F. Temurtaş, "An experimental study on sensorless determination of the projectile position by artificial neural network in magnetic launcher systems," *IEEE Transactions on Plasma Science*, vol. 49, no. 12, pp. 3970–3979, Nov. 2021. https://doi.org/10.1109/TPS.2021.3123064

[19] B. Zhang, Y. Kou, K. Jin, and X. Zheng, "A multi-field coupling model for the magnetic-thermal-structural analysis in the electromagnetic rail launch," *Journal of Magnetism and Magnetic Materials*, vol. 519, Feb. 2021, Art. no. 167495. https://doi.org/10.1016/j.jmmm.2020.167495

[20] T. Li, G. Feng, C. Du, and P. Zhang, "Analysis of electromagnetic characteristics of copper-steel composite quadrupole rail," *Materials*, vol. 15, no. 17, Aug. 2022, Art. no. 5851. https://doi.org/10.3390/ma15175851

[21] D. Ceylan, M. Karagöz, Y. Çevik, B. Yıldırım, H. Polat, and O. Keysan, "Simulations and experiments of EMFY-1 electromagnetic launcher. *IEEE Transactions on Plasma Science*, vol. 47, no. 7, pp. 3336–3343, May 2019. https://doi.org/10.1109/TPS.2019.2916220

[22] M. P. Galanin, A. K. Kondratenko, V. V. Lukin, A. S. Rodin, and D. L. Sorokin, "Methods of numerical modeling of a railgun with magnetization turns," *Journal of Engineering Physics and Thermophysics*, vol. 92, pp. 820–828, July 2019. https://doi.org/10.1007/s10891-019-01991-x

[23] B. Cheng, "The development of a novel coil gun with permanent magnet," in *2023 IEEE/ASME International Conference on Advanced Intelligent Mechatronics (AIM)*, Seattle, WA, USA, June 2023, pp. 531–536. https://doi.org/10.1109/AIM46323.2023.10196246

[24] P. Stone, "Electromagnetic launcher," in *2021 IEEE Pulsed Power Conference (PPC)*, Denver, CO, USA, Dec. 2021, pp. 1–5. https://doi.org/10.1109/PPC40517.2021.9749836

[25] H. Chen, Y. Zhan, R. Nie, and S. Zhao, "Multiobjective optimization design of tubular permanent magnet linear launcher," *IEEE Transactions on Plasma Science*, vol. 47, no. 5, pp. 2486–2492, Feb. 2019. https://doi.org/10.1109/TPS.2019.2896886

[26] N. M. Noor, I. Aris, N. Misron, S. Shafie, and P. Iqbal, "Performance analysis of the linear launcher motor via modelling and simulation for light electric vehicles," *Pertanika Journal of Tropical Agricultural Science*, vol. 29, no. 1, Jan. 2021. https://doi.org/10.47836/pjst.29.1.05

[27] F. W. Grover, "Formulas and tables for the calculation and design of single-layer coils," *Proceedings of the Institute of Radio Engineers*, vol. 12, no. 2, pp. 193–208, Apr. 1924. https://doi.org/10.1109/JRPROC.1924.219955

[28] D. Yang, Z. Liu, T. Shu, L. Yang, and J. Ouyang, "Design and testing of a coil-unit barrel for helical coil electromagnetic launcher," *Review of Scientific Instruments*, vol. 89, no. 1, Jan. 2018. https://doi.org/10.1063/1.5001882

[29] M. T. Bhoskar, M. O. K. Kulkarni, M. N. K. Kulkarni, M. S. L. Patekar, G. M. Kakandikar, & V. M. Nandedkar, "Genetic algorithm and its applications to mechanical engineering: A review," *Materials Today: Proceedings*, vol. 2, no. 4–5, pp. 2624–2630, 2015. https://doi.org/10.1016/j.matpr.2015.07.219